LITE Measurements of Sea Surface Directional Reflectance and the Link to Surface Wind Speed

Robert T. Menzies[1], David M. Tratt[1], and William H. Hunt*

‘Jet Propulsion Laboratory, California Institute of Technology, Pasadena, California91109

[2]Wyle Laboratories, Hampton, Virginia 23666

Abstract

The dependence of sea surface directional reflectance on surface wind stress suggests a method for deriving surface wind speed from space-based lidar measurements of sea surface backscatter. in particular lidar measurements in the nadir angle range from 10-30 degrees appear to be most sensitive to surface wind speed variability in the regime below 10 m/s. The LITE shuttle lidar mission of September, 1994 provided a unique opportunity to measure directional backscatter at selected locations, using the Landmark Track maneuver, and to measure fixed-angle backscatter from the ocean surfaces on a global scale. During the Landmark Track maneuver the shuttle orbiter orientation and roll axis are adjusted continuously to maintain the lidar footprint at a fixed location for a duration of about one minute. Several datasets have been converted to calibrated reflectance units and compared with a surface reflectance model to deduce surface wind speeds. Comparisons have been made with ERS- 1 scatterometer data and surface measurements.

Keywords:

Introduction

The angular dependence of the sea surface reflectance depends strongly on the surface winds (commonly referenced to a height 10 m above the surface), which determine the surface wave structure. At low and moderate surface wind speeds the surface reflectance depends primarily on the slope distribution of the capillary and capillary-gravity wave facets superimposed on the longwave swells [1-4]. The reflectance characteristics depart significantly from those of the ideal diffuse Lambertian surface, falling off much more rapidly with increasing nadir angle. At higher surface wind speeds the contributions from foam (whitecaps) and spray alter the angular reflectance properties [5,6]. In the visible subsurface scattering can also contribute, becoming relatively more important at larger nadir angles [7-9].

The departure of the reflectance angular distribution from Lambertian behavior is important for several reasons. For example it plays a role in emissivity modeling at IR (infrared) wavelengths, affecting the ability to recover accurate sea surface temperatures and cloud optical thicknesses from satellite IR radiometer data [1 O- 12]. For lidar measurement applications the size and dynamic range of the retroreflectance vs. off-nadir angle is important for performance evaluations of future scanning Earth-orbiting lidars such as Doppler wind lidars [13-15]. The degree to which the surface reflectance signal can be distinguished from the boundary layer aerosol signal at the large off-nadir angles can impact aspects of data analysis and calibration and alignment verification. Establishing a robust link between the angular distribution function and the surface wind speed permits the potential for scanning backscatter lidar measurement of surface winds as well as boundary layer thickness and aerosol optical depth, and for enhancement of Doppler wind lidar measurements of marine boundary layer wind profiles.

Only a few attempts have been made to investigate quantitatively the angular dependence of sea surface reflectance using the lidar technique. Although numerous airborne lidars exist, they are predominantly used in a nadir or near-nadir fixed pointing mode. (A notable exception is the Large Aperture Scanning Airborne Lidar (LASAL) instrument which has flown on the NASA P3-B aircraft [16], primarily for boundary layer studies.) Early measurements of laser backscatter from a wind-driven water surface were made by Petri [17], using a modulated cw Nd:YAG laser system operating at a wavelength of 1.06 µm. He mounted the apparatus on a platform suspended beneath the Chesapeake Bay Bridge near Annapolis, Maryland and recorded signals over an angular scan range of+/- 37.5 degrees from nadir. The platform was about 20 m above the surface, and the laser footprint diameter ranged from 15-30 cm over the scan range. In the early 1980's Bufton et al. [18] reported a series of six angular profiles using the NASA airborne oceanographic lidar (AOL) off the coast of Maryland. In addition to the profiles at the 532 nm and 337 nm wavelengths of the AOL, a few measurements of surface backscatter were obtained with a carbon dioxide laser system on the same aircraft, at 9.5 µm wavelength. The footprint diameters varied from 40 cm to about 10 m. A review of ocean surface scattering models was included in [18], and comparisons were made with model predictions.

The Lidar In-space Technology Experiment (LITE) consists of a three-wavelength backscatter lidar developed by the NASA Langley Research Center to fly on the Space Shuttle, with measurement objectives including cloud heights and spatial structure, aerosol layer heights and backscattering ratios, and selected case studies of land and ocean (retro)reflectances [19]. LITE flew in September 1994 on the STS-64 mission, and a description of the instrument, flight operations, and selected data products can be found in reference [20]. Since both the backscatter signals and the background radiances collected by a downward-viewing lidar receiver in Earth orbit can vary over a wide dynamic range, LITE was designed to handle a variety of uplink commands to configure the optical bandwidths, fields-of-view, and receiver gains according to the particular primary scientific objective at a particular time during the mission. The nominal pointing configuration was 5-degrees off nadir. This deviation from nadir-pointing was chosen to substantially reduce specular reflection effects from e.g., smooth water surfaces. The LITE transmitter footprint on the surface, at its nominal 250 km altitude depended on wavelength. At the 1064 nm, 532 nm, and 355 nm transmitted wavelengths, the footprint diameters were 420m, 280m, and 240 m respectively at the 5° nadir angle. The orbit inclination was 57°, the daytime Equator crossing being from south to north.

Measurement Description

On six occasions during the LITE shuttle lidar mission in September 1994 the orientation of the Shuttle Discovery was maneuvered in order to permit measurements of the lidar backscatter from a selected patch of sea surface over a continuous range of nadir angles, a manuever called the "Landmark Track”. Each was conducted during daylight conditions to allow the astronauts to assess the cloud conditions immediately prior to reaching the target areas. The Landmark Track maneuver involved setting the orientation of the shuttle such that the lidar pointed ahead, directly over the suborbital track, at a fixed nadir angle of -30 degrees, holding that orientation until the astronauts gave a go-ahead to proceed, and then commanding the shuttle orientation to follow a pre-programmed roll in order to maintain the lidar footprint over a fixed location until the nadir angle reached +30 degrees. The lidar footprint wander at the sea surface during the maneuver was less than 3 km, corresponding to the level of accuracy of shuttle attitude control during the angle sweep. During the post-mission data analysis the time-of-flight of the pulse to the surface was used to calculate the nadir angle vs. time during the maneuver. This proved to be a more accurate means of obtaining the true nadir angle because the shuttle orient ation in the orthogonal axis was occasionally found to be 2-2.5° off-nadir.

Over the nadir angle range +/- 30 degrees several orders of magnitude dynamic range were expected, and were indeed encountered under calm sea surface conditions. The instantaneous dynamic range of each of the LITE channels was relatively limited, particularly during daylight conditions when it was necessary to subtract a background offset due to the upwelling background radiances (scattered sunlight) in each of the three spectral bands. During the first three Landmark Tracks the gain was adjusted to maximize the lidar sensitivity to the low backscatter signals expected from the large nadir angles, at the risk of saturating the receivers during the near-specular portion of the scan. The rationale was that very little lidar sea surface backscatter data existed at angles beyond a few degrees off nadir, consequently obtaining those data should receive higher priority. During the mission the NASA Langley LITE engineering team implemented the use of command sequences which changed gain settings at the appropriate times during the Landmark Tracks, from high gain at the larger nadir angles to reduced gain in the neighborhood of nadir. Two of the six Landmark Tracks were repeats over the same target areas due to problems with the selected instrument configuration settings during the first attempts. Of the remaining four, two were located in the equatorial region, the first in the Atlantic Tradewinds area and the second in the Eastern Pacific, The other two were located in the Gulf of California and in Lake Superior. The locations are listed in Table 1 in chronological sequence.

The LITE measurements were taken during low to moderate surface wind conditions and provide a means of testing ocean surface models which link capillary and capillary-gravity wave slope distribution to surface wind speed without the complications which arise when attempting to model a heavy sea state.

An effort was made to use the LITE surface backscatter signals to deduce absolute values of surface backscatter as well as angular dependence. Pre-flight atmospheric tests at NASA Langley Research Center established calibrations at the 355 nm and 532 nm channels, using the backscattering ratio technique. Establishing the calibration for the 1064 nm channel required comparisons of each of the lidar transmitter and receiver responsivity factors in the 1064 nm channel with those of the 532 nm channel, then comparing the calculated result with the two-wavelength reflectance measurement comparisons over relatively calm open ocean surfaces, at the nominal fixed nadir angle of 5 degrees selected for the mission. The 532nm/1064nm reflectance ratio over such surfaces at small nadir angles, when whitecap and subsurface scattering contributions are relatively insignificant, should be given by the Fresnel reflectance ratio, which is well characterized, The calculated result agreed very well with these measurement results, providing a degree of confidence in the 1064nm calibration. The difference between calculated and measured ocean surface reflectance was slightly less than 2%, while the measurement uncertainty was estimated to be +/- 3%.

The Landmark Tracks (LMT's) required a unique receiver configuration, making it necessary to uplink a special set of commands prior to each LMT. A mission objective was to digitize the lidar backscatter signals over a time period which includes a "background only" component (e.g., from sufficiently high altitudes such that the molecular and aerosol backscatter are below the receiver noise levels) and extending to a few km beyond the surface return range. The digitization period for the 355 nm and 532 nm channels was 550 μs, corresponding to a total range depth of 82.5 km. The onboard data storage and downlink data rate capacity resulted in choosing an abbreviated time period for which the 1064 nm receiver digitizers operated. Because the range to the surface varied by more than 40 km during a typical LMT scan, it was required to adjust the digitization time periods, a particularly critical adjustment for the 1064 nm channel. It was also necessary to adjust the receiver gains of each of the three channels in order to maintain surface return signals above the receiver noise levels at the large nadir angles yet avoid saturation near nadir. It proved to be extremely difficult to accomplish this with three fixed gain settings; consequently a special set of commands were implemented for the later LMT opportunities which resulted in automatic gain changes during the LMT maneuvers.

Ocean Surface Reflectance Model

The LITE LMT data have been compared with predictions based on a surface wind dependent model of wave specular reflectance [1,3,4] supplemented by the contribution from foam [5,6] and from underwater backscatter [7-9]. The total backscatter, or retroreflectance, can be written as

$$R = W \cdot R_{f,eff} + (1-W) \cdot R_s + (1-W \cdot R_{f,eff}) \cdot R_u \ , \tag{1}$$

the first term being the contribution from foam patches, i.e., the product of the fraction of the surface covered with whitecaps, W, and the effective reflectance of the whitecaps; the second term being the specular reflectance of the surface waves on the fraction of the water surface which is not covered by foam; and the third term describing the volume backscattering from the water molecules and suspended material in the water, for those wavelengths which penetrate into the water. This form was used by Koepke [5], where he referred to R_u in the third term as the underlight. Koepke made the assumption that the reflectance of the foam patches is the same for incident light coming from above or below the surface, hence the bracketed factor in the third term. In the lidar case we interpret the third term as backscattered light from beneath the surface which appears only during the short time period when the lidar receiver is sampling signals from that range (The sampling rate of each digitizer in the LITE receiver was 10 MHz, corresponding to range increments of 15 m, and the surface reflectance signal was calculated by summing over 150 m on either side of the range location of the peak signal. This process includes nearly all the backscatter from beneath the surface, since an attenuation length at the most transparent wavelengths is typically less than 100 m in the ocean waters.)

Discounting foam (whitecaps) and subsurface backscatter for the moment, the ocean surface can be modeled as a number of specular wave slopes, and the optical reflectance pattern is dictated by their slope distribution. The wind-driven ocean surface waves which contribute to optical scatter at off-specular angles can be viewed as capillary waves, capillary-gravity waves (over the intermediate scales for which both the gravitational and surface tension forces are significant), and short gravity waves in the wave number range $k = 2\pi/\lambda$ between 10^{-1} and 5×10^{1} cm^{-1}, which ride on the longer gravity waves that provide overall tilt to the surface [21,22]. The facets of capillary waves, for which viscous dissipation is predominant, exist at scales as small as 1 mm. This is still large compared with optical wavelengths, so that diffraction effects are not important (in contrast with the scattering models appropriate for radar wavelengths), and geometric optics provide a satisfactory interpretation.

Cox and Munk [1] concluded from their sun glitter observations that the tilted specular facets produced by the surface waves could be described well as a Gaussian probability distribution of facet slopes, although there was some skewness associated with the upwind-downwind direction which increased with increasing wind speed. The LITE observations are in the low wind speed regime, and we assume a Gaussian distribution of sloped facets, with each facet providing specular reflectance. The surface wave slope variance has been linked to surface (10-m height) wind speed via a power law or a logarithmic dependence.

$$p(z_x, z_y) = (\pi\langle s^2\rangle)^{-1} \exp-((z_x^2 + z_y^2)/\langle s^2\rangle) \qquad (2)$$

where $z_x = \partial z/\partial x$, $z_y = \partial z/\partial y$, are the 2-dimensional slope components, and $\langle s^2\rangle$, is the total mean-square slope variance. Cox and Munk [1] expressed the mean-square slope dependence on wind speed (as measured at a height of41 ft. (12.4 m) above sea level) as a 2-term power series, a constant plus a linear term, with the linear term dominating for wind speeds at 2 m/s and greater. Cox and Munk noted that the observed variance of the upwind/downwind slope component was usually somewhat larger than that of the crosswind slope component. They provided expressions for the upwind/downwind and crosswind components of the slope variance, as well as the total slope variance, although at wind speeds of 5 m/s or less, the associated uncertainty levels mask the distinction between upwind /downwind vs. crosswind variances. Wu [4] reanalyzed the Cox and Munk [1] data, first transferring to a wind speed at the standard 10-m height assuming a standard logarithmic profile, then fitting the total mean-square slope vs. wind speed data using a two-branch logarithmic fit:

$$\begin{aligned} \langle s^2 \rangle &= (\ln U_{10} + 1.2)10^{-2}, \qquad U_{10} \leq 7 \ m/s, \\ &= (0.85 \ln U_{10} - 1.45)10^{-1}, \ U_{10} > 7 \ m/s \ . \end{aligned} \tag{3}$$

These correspond to two hydrodynamic regimes: a regime below 7 m/s where capillary waves are weakly developed, and a region above about 7 m/s where capillaries are increasingly developed. Eqn. (3) slope variances depart from those derived from the Cox and Munk expression for low wind speeds, well below 5 m/s. An example will be shown later. The Cox and Munk data also indicate a substantial reduction of<<> in the wind speed range 2-10 m/s over an oil slick, where it was noticed that waves with lengths of less than about 30 cm were significantly suppressed.

We use the formulations of Kodis [23] and Barrick [24] to calculate laser backscatter based on the surface slope distribution and the Fresnel reflectance of the air-water interface, in a manner similar to that described in Bufton et al. [18], and by Tsai and Gardner [25] in computing the temporal moments of the received signal from a nadir-pointing laser altimeter. The Fresnel reflectance is a slowly varying function of wavelength over the LITE wavelength range, with the value at 532 nm equal to 0.020. Refractive index data from Hale and Querry [26] were used to compute the values at the three LITE wavelengths. (Adjustments to the refractive index for the seawater case (compared with pure water) were reported by Friedman [27] for wavelengths beyond 1.5 pm. The Hale and Querry data are assumed to be adequate for the LITE data.) Kodis [23] indicated that the mean backscatter can be described in terms of the average number of specular glints on the surface multiplied by the average curvature (product of the principal radii of curvature) at these points. Barrick [24] derived expressions for both quantities, making assumptions that the radii of curvature were much greater than the wavelength and that the slopes were Gaussian distributed. He then derived an expression for the (dimensionless) backscatter cross section per unit surface area, o". Normalization by 2π sr yields the lidar backscatter, R_s (sr^{-1}) from the waves on the wind-roughened surface as a function of nadir angle θ,

$$R_s = \frac{p \sec^4\theta}{2\pi\langle s^2\rangle} \exp\left(- \frac{\tan^2\theta}{\langle s^2\rangle}\right), \qquad (4)$$

where p is the Fresnel reflectance. (This expression is a factor of two larger than the equivalent in Bufton, et al. [18]. Since Barrick [24] derived a backscatter cross section per unit surface area, it should be normalized by 2π rather than the 4π used by Bufton, et al. [18].)

More recent observations have indicated that atmospheric stability effects on the surface wave slope statistics must be considered. Hwang and Shemdin [28], using a refractive laser slope gauge mounted on an ocean tower structure, observed departures from the Cox and Munk dependence of the mean square slope on wind speed under conditions for which the stability of the atmospheric surface layer departed from neutral stability. Most of their observations were taken for neutral and positive stability situations, with the result being a decrease in mean square slope for a given wind speed approaching asymptotically a factor of nearly 2 for strong positive stability (air temperatures warmer than water temperatures), compared with the neutral stability case. Recently Shaw and Churnside [29] reported observations in negative stability regime, demonstrating increasing relative mean-square slope with increasing negative stability. Their relative mean-square slope (normalized by the Cox and Munk values) for the standard 10-m height surface wind ranging from 4-10 m/s reached values of 2 for the largest observed values of negative stability; however there was no evidence of a saturation, or asymptotic value, of the relative mean-square slope in contrast with the observations in the positive stability regime.

The LITE Landmark Track data discussed here include locations in open ocean in the tropical zones of the Atlantic and Eastern Pacific, where stability is expected to be neutral. For the two other cases presented here, atmospheric stability may have been moderately positive and could have been a factor.

Koepke [S] presents the spectral dependence of the effective reflectance of oceanic foam, using the reflectance data of fresh, dense foam as measured by Whitlock et al. [6], and relationships between surface wind speed and the fractional coverage factor, *W*, in Eqn. (1). The fractional coverage factor is zero for wind speeds below 5 m/s. It increases from O. 1% to 1% in the wind speed range 5- 10 m/s. The foam is assumed as a diffuse, Lambertian reflectance source.

We have not attempted to model the subsurface reflectance term in Eqn. (1); however it does contribute significantly to the LITE sea surface reflectance at the large nadir angles for both the 355 nm and 532 nm wavelengths, as discussed in the next section. The subsurface reflectance depends on the presence of phytoplankton and suspended inorganic and/or inorganic particulate matter and can vary over a wide dynamic range. Morel and Prieur [7] and Morel [8] summarize data on subsurface scattering based on a large number of measurements in various types of waters. Gordon and Morel [9] point out that the scatter from the water column which is penetrated by the light can be treated as a Lambertian reflector essentially at the surface, the reflectance ρ^s_U obtained by means of a measurement of the subsurface irradiance ratio. In clear open ocean waters, in the mid-visible, p^s~(532 nm) values range from several tenths of a percent to about two percent [7]. The equivalent lidar backscatter is $(\rho^s_U/\pi)\cos\theta$, for nadir angle θ.

Disregarding for the moment the existence of upwind-crosswind slope variance differences and using the total slope variance as in Eqn. (3), the modelled lidar backscatter from the sea surface and its dependence on nadir angle is given in Figure 1 for various surface wind values, Contributions from the third term of Eqn. (1) are not included. On this plot the foam contribution is evident only for the surface wind speeds 8 m/s and 10 m/s, producing the much flatter Lambertian angular dependence at the larger nadir angles. The curves of $d\log R/dU_{10}$ for the surface wind speed range O - 15 m/s and various incidence angles are shown in Figure 2. One can see that the fractional change in lidar reflectance is quite small over this range of wind speeds for angles less than 5°. For incidence angles between 10 and 30 degrees, there is significant sensitivity to wind speed variation for wind speeds up to 7-8 m/s, the 10-20 degree range of incidence angles being particularly sensitive to small variations at low (<5 m/s) wind speeds,

Validation Data

Data from the ERS- 1 scatterometer were used to support the landmark track studies in the tropical Atlantic and Pacific oceans. Additional data were obtained from the Gulf of California based on surface stations in Baja California, and from Lake Superior based on ship wind reporting. These data indicated surface winds under 10 m S-l in all locations. The low to moderate wind speeds simplify the comparisons with model predictions, for complications such as shadowing and multiple glint reflections become increasingly important at higher wind speeds and larger nadir angles [30].

Measurement Results

LITE was launched aboard the Space Shuttle Discovery on September 9, 1994. As stated earlier the anticipated large dynamic range of lidar backscatter signals from the sea surface over a nadir angle range from O -30 degrees was expected to be more than the LITE receiver dynamic range could handle with fixed gain settings. Highest priorit y was given to the study of the surface backseat ter at the larger nadir angles, sacrificing data at the small nadir angles to potential signal saturation.

On September 12 (Day 255) a Landmark Track was executed over the tropical Atlantic Ocean, in the trade winds belt, and another was executed in the Gulf of California. The ERS- 1 scatterometer data in the region of the Atlantic trades Landmark Track, taken 7 hrs. after the LITE overpass, indicated northeasterly winds with wind speed in the 2.5 - 4 m/s range. Scattered clouds were in the neighborhood of the Atlantic Landmark Track location, but it was decided to go ahead and execute the maneuver at the planned time and location. Unfortunately the data for positive nadir angles (aft view) larger than 12° were lost due to a Ku band telemetry problem, and signal saturation from the sea surface back scatter occurred for nadir angles less than 60 at both the 532 nm and 1064 nm channels. The data from the 532 nm and 1064 nm channels both indicated sporadic signal levels consistent with a 5 m/s surface wind model prediction, but with significant surface signal depression over several segments of the scan, the most severe 'dip' being centered at -14°. A search indicated no clouds in the FOV for these segments. The 1064 nm signal level dropped to the receiver noise level in these segments of the scan, while the 532 nrn signal level dropped to the level of the subsurface volume backscatter (which can be determined by viewing the 532 nm signals at the large nadir angles). This would be consistent with an encounter with patches of oil slick or a natural surface film on the surface, suppressing the shorter surface waves which contribute to off-nadir surface backscatter. However this is speculation, and the data are not useful for drawing any conclusions.

The Gulf of California location was selected because of the high probability of clear weather. The nearest surface wind reports that we were able to retrieve, from Ensenada, indicated light, variable winds from O-5 m/s near the orbit 50 overpass time on September 12. The Landmark Track during orbit 50 was only marginally successful, due to problems associated with the selection of the LITE parameters during the pre-maneuver setup. The 1064 nm surface signal data were lost due to an incorrect digitization time delay setting. The 532 nm channel gain setting was inappropriate for the Landmark Track, resulting in surface return signal saturation *over* the useful range of nadir angles. The 355 nrn data are shown in Figure 3. The negative angle (forward view) data are folded onto the positive side in order to visually assess the degree of asymmetry. Signal saturation occurred over the central +/- 5°. The instrument noise level was equivalent to a surface backscatter of 10-2 sr'. The signal dynamic range was limited to one order of magnitude at 355 nm due to large Rayleigh scattering loss and because of the need to subtract a substantial background signal level from the atmosphere. These data indicate very low surface wind speed and substantial asymmetry in the positive and negative nadir angle portions of the sweep, the negative angle data decreasing more rapidly with increasing nadir angle. An upwind-downwind asymmetry at higher wind speeds was noted by Cox and Munk [1] and by Shaw and Churnside [29] in that fits to both of their datasets were improved by adding a skewness coefficient to the Gaussian. Data are sparse at such low wind speeds, however. The two model curves shown in Figure 3 are each for a 2 m/s wind speed, The Wu [4] curve is based on the total slope variance of Eqn. (3), while the C&M curve is based on the upwind slope variance of Cox and Munk [1]. (Cox and Munk observed no discernible difference between upwind and crosswind slope variances at such low wind speeds as 2 m/s.) At this wind speed the two slope variances differ by a factor of three, thus the Wu curve duplicates a C&M curve which would be obtained using a 6 m/s wind speed. At the smallest nadir angles for which we have data, the data appear to fit the C&M model for 2 m/s wind speed, although as the nadir angle increases there is a substantial divergence, and the aft-looking data become consistent with a slope variance a factor of three larger. Shortly after this orbit 50 Landmark Track it was decided to execute another Landmark Track over the Gulf of California later in the mission.

The data from the tropical eastern Pacific Landmark Track on September 14 (Day 257) were more encouraging. Widely scattered cumulus ('popcorn') clouds were noticed in the area by the astronauts. The ERS-I scatterometer data indicated primarily easterly winds in the 4-4.5 m/s range, with a small (-2 -3 m/s) southerly component which the scatterometer could not retrieve with much accuracy. The LITE data are shown in Figures 4 and 5 for the 1064 nm and 532 nm wavelengths, respectively. As before, the data from each side of the Landmark Track scan are folded together in each plot, and in this case there is no detectable asymmetry. Signal saturation occurred at nadir angles below 8° for the 1064 nm data, and below 120 for the 532 nm data, The model curves shown in Figures 4 and 5 are based on the slope variance of Eqn. (3). At 5 m/s wind speed this slope variance is about a factor of two larger than the Cox and Munk [1] upwind slope variance, thus the use of the latter would require a 10 m/s surface wind speed to fit the data. The 1064 nm data closely follow the model curve for 5 m/s over the applicable range of nadir angles. The 1064 nm signal drops to the receiver noise level in the neighborhood of 20°. The dip near 10 nadir angle from one side of the scan is due to partial cloud attenuation on the backward look angle side of the maneuver. The degree to which the 532 nm data fit the 5 m/s model curve is inconclusive, because subsurface volume backscatter begins to dominate for angles greater than 160. The equivalent Lambertian reflectance from the subsurface scattering is $\rho^{s}_{L} = 1\text{-}\ 1.5\,\%$.

On September 16 Landmark Tracks were executed over the Gulf of California and Lake Superior. For these cases a special command sequence was telemetered to LITE just prior to the maneuvers which resulted in automatic gain changes, reducing the gain for the small nadir angle range in order to avoid receiver saturation from the relatively high backscatter signals. Surface wind reports from Baja California indicated winds between 5- 10 m/s. There were no ship reports available. Ship winds available from Lake Superior indicated 5-7 m/s wind speeds in the late afternoon of September 16.

For the Gulf of California Landmark Track Figures 6 and 7 show the results for the 1064 nrn and 532 nm wavelengths, respectively. The 1064 nm data follow the curvat ure of the model curves (which use the Eqn. (3) expression for slope variance) for the 5-6 m/s surface wind speed range until the signals reach the receiver noise level at nadir angles beyond 200. For the 532 nm case, although the backscatter level agrees with the model for small nadir angles, the shape of the curve deviates from the Gaussian model for angles of 5° and greater. The Eastern Pacific data of Figure 5 suggest the same type of deviation at the smallest nadir angles for which data are available. The effective Lambertian reflectance at 532 nm from subsurface volume backscatter is near 1.5°/0. It can be seen that there is very little asymmetry at either wavelength.

Lake Superior was a target of opportunity, as the orbit 113 suborbital track which crossed over the Gulf of California also crossed over it during clear weather. The reflectance data from the Lake Superior Landmark Track are shown in Figures 8 and 9. The angular dependence are clearly uncharacteristic if the surface wind speed was in the 5-7 m/s range, First the reflectance decreases much more rapidly with increasing nadir angle than the 5 m/s model curves for each wavelength. Second, there is detectable asymmetry, the curves for forward and backward looking angles being individually discernible. Two potential causes are (1) an oil slick or film on the surface, and (2) positive stability in the atmospheric surface layer. Hwang and Shemdin [27] noted that the effect of the latter was to decrease the mean square wave slope; however, their data indicate that as the stability becomes increasingly positive, the reduced mean square slope reaches an asymptotic limit at a value of 0.5 times that expected for neutral stability. The data indicate a more dramatic reduction in mean square slope. Cox and Munk [1,3] observed that for the wind speed regime< 10 m/s an oil slick reduced the wind-dependent contribution to the mean square slope by a factor of more than 3, and waves shorter than 30 cm were reported to be absent. There was no surface sampling in the area at the time of the LITE overpass to assist in understanding the cause of this behavior. We observe that the underwater volume backscatter at 532 nm is equivalent to a Lambertian reflectance parameter of 1 %, 60-70% of that observed in the Gulf of California.

Discussion

The LITE Landmark Tracks are the first attempt to study the angular dependence of laser reflectance from the sea surface using a space-based lidar. Data were collected at locations several tens of km to several hundred km from coastal zones, over a continuous range of nadir angles out to 30°. The large transmit ter footprints (particularly at the 1064 nm wavelength) resulted in instantaneous averaging over the complete range of the surface wave spectrum which contributes significantly to mean square slope. The impact of the large footprints must be stressed, for a Landmark Track maneuver using a lidar with much smaller transmitter divergence would likely result in a signal substantially modulated by the swell as the nadir angle varied. Hoge et al. [31], collected sea surface reflectance data from an airborne lidar with a footprint of about 1 m diameter, in the case of a swell-dominated sea with low (5m/s) surface wind speed. The lidar data indicated large surface height and backscatter variability at surface wavelengths up to 200 m. It was also noted that the wave crests provided higher backscatter than the troughs. This is consistent with the wave tank observations of Cox [2] that the capillary waves are more evident near the crests than in the troughs of the longer waves.

Coincidentally the surface winds at the various Landmark Track locations were very nearly the same, i.e., 4-7 m/s based on ERS - 1 satellite scatterometer and surface observations. Although the datasets are very limited in number, and by coincidence the range of surface wind speeds was very restricted, several comments can be made from the data.

As expected, the 1064 nm wavelength was much better suited to observation of the wide dynamic range of surface scattering due predominantly to capillary and capillary-gravity waves in the low surface wind speed regime. Indications are that, with the exception of the Lake Superior case, the 1064 nm data could be fit well with the described model. At the 532 nm wavelength, subsurface volume backscatter was a significant contributor to the signal for nadir angles larger than 15°, resulting in a much flatter dependence of lidar backscatter on nadir angle. The same was true for the 355 nm wavelength; in addition, the significant atmospheric extinction due to Rayleigh scattering at 355 nm reduced the available dynamic range. With the exception of the first Gulf of California pass, where the winds were very light and the location was less than 50 km from the north end of the Gulf, very little skewness was observed, although significant deviations from the Gaussian shape are apparent for the 532 nm and 355 nm data. We *were* not able to validate the foam contribution to the model due to the low surface wind speeds and the limited LITE 1064 nm receiver sensitivity during the daytime conditions when all the Landmark Tracks occurred.

It appears that with the LITE 1064 nm wavelength sea surface backscatter characteristics being in good agreement with a rather simple model of surface wave reflectance in the low wind speed regime, it can be stated that space lidar sea surface backscatter measurements over a range of nadir angles between 10° and 25” are a sensitive indicator of surface wind speed in the low wind speed regime. Weinman [32] proposed the use of backscatter lidar signals at 15° nadir angle to retrieve surface wind speed. The model curves in Figure 2 and the bulk of the LITE data indicate that, with sufficient lidar sensitivity, a 20°-25’ nadir angle would be more sensitive over the range of wind speeds considered here, with multiple look-angle data over the 10° -30 range being optimal. The ability to resolve wind speed variability at the ± 1 m/s level is potentially within the capability of a calibrated backscatter lidar, and further experimental studies of the angular dependence of lidar backscatter from the sea surface are highly desirable. Coincident surface observations of e.g., wind speed and direction, stability of the surface layer, and any presence of surface films are essential in gaining an improved slope variance model for use with backscatter lidar observations.

Acknowledgements

The authors would like to acknowledge the NASA Langley LITE Project, Drs. M.P. McCormick and D.M. Winker of NASA Langley Research Center for their efforts in arranging the Landmark Track maneuvers in the LITE flight plans, Dr. C. Gardner for fruitful technical discussions and provision of the Lake Superior surface wind data, and A. Brothers of JPL for data analysis contributions. This work was carried out by the Jet Propulsion Laboratory, California Institute of Technology, under contract with the National Aeronautics and Space Administration.

References

1. C. Cox and W. Munk, 'Measurement of the Roughness of the Sea Surface from Photography of the Sun's Glitter', J. Opt Sot. Am. 44, 838-850 (1954).

2. C. Cox, ' Measurements of the Slopes of High Frequency Wind Waves', J. Marine Res. 16, 199-225 (1 958).

3. C. Cox and W. Munk, 'Statistics of the Sea Surface Derived from Sun Glitter', J. Mar.Res. 13, 198-227 (1954).

4. J.Wu, 'Sea-Surface Slope and Equilibrium Wind-Wave Spectra', The Physics of Fluids, Vol 13, No. 5 (1972).

5. P. Koepke, 'Effective Reflectance of Oceanic Whitecaps', Appl. Opt. 23, 1816-1824 (1984)

6. C.H. Whitlock, D.S. Bartlett, and E.A. Gurganus, 'Sea Foam Reflectance and Influence on Optimum Wavelength for Remote Sensing of Ocean Aerosols', Geophys. Res. Lett. 9,719-722 (1982).

7. A. Morel and L. Prieur, 'Analysis of Variations in Ocean Color', Limnol, Oceanogr, 22, 709-722 (1977).

8. A. Morel, 'In-water and remote measurements of ocean color', Boundary Layer Meteorol. **18,** 177-201 (1980).

9. H. R. Gordon and A.Y. Morel, *Remote Assessment of Ocean Color for Interpretation of Satellite Visible Imagery: A Review* (Springer-Verlag, New York, 1983).

10. K. Masuda, T. Takashima, and Y. Takayama, 'Emissivity of pure and sea waters for the model sea surface in the infrared window regions', Remote Sensing Environ. 24, 313-329 (1 988).

11. J. Otterman, J. Susskind, G. Dalu, D. Kratz and I.L. Goldberg, 'Effects of Water Emission Anisotropy on Multispectral Remote Sensing at Thermal Wavelengths of Ocean Temperature and of Cirrus Clouds', Appl. Opt. 31, 7633-7646 (1992).

12. X. Wu and W.L. Smith, 'Emissivity of rough sea surface for 8-13 pm: modeling and verification', Appl Opt. **36**, 2609-2619(1997).

13. R.M. Huffaker, T.R. Lawrence, M.J. Post, J.T. Priestley, F.F. Hall, Jr., R.A Richter, and R.J. Keeler, "Feasibility studies for a global wind measuring satellite system (Windsat): analysis of simulated performance", Appl. Opt. 23,2523-2536 (1984).

14. R.T. Menzies and R.M. Hardesty, "Coherent Doppler lidar for measurements of wind fields", Proc. IEEE 77,449-462 (1989).

15. W.E. Baker, G.D. Emmitt, F. Robertson, R.M. Atlas, J.E. Molinari, D.A. Bowdle, J. Paegle, R.M. Hardesty, R.T. Menzies, T.N. Krishnamurti, R.A. Brown, M.J. Post, J.R. Anderson, A.C. Lorenc, and J. McElroy, "Lidar-measured winds from space: a key component for weather and climate prediction", Bull. Amer. Meteor. Sot., 76, 869-888 (1995).

16. S.P. Palm, S.H. Melfi, and D.L. Carter, 'New Airborne Scanning lidar System: Applications for Atmospheric Remote Sensing', Appl. Opt. 33,5674-5681 (1994).

17. K.J. Petri, 'Laser Radar Reflectance of Chesapeake Bay Waters as a Function of Wind Speed', IEEE Transactions on Geoscience Electronics, Vol. GE-15, No. 2 (1977).

18. J.L. Bufton, F.E. Hoge, and R.N. Swift, 'Airborne Measurements of Laser Backscatter from the Ocean Surface', Appl. Opt. 22,2603-2618 (1983)

19. M.P. McCormick, D.M. Winker, E.V. Browell, J.A. Coakley, C.S. Gardner, R.M. Hoff, G. S. Kent, S.H. Melfi, R.T. Menzies, C.M.R. Platt, D.A. Randall, and J.A. Reagan, "Scientific invest igat ions planned for the Lidar In-space Technology Experiment (LITE)", Bull. Amer. Meteor. Sot. 74,205-214 (1993).

20. D.M. Winker, R.H. Couch, and M.P. McCormick, "An overview of LITE: NASA's Lidar In-space Technology Experiment", Proc. IEEE 84, 1-17 (1996).

21. O.M. Phillips, *The Dynamics of the Upper Ocean*, 2nd edition (Cambridge University Press, London, 1977).

22. M.A. Donelan and W.J. Pierson, Jr., 'Radar scattering and equilibrium ranges in wind-generated waves with application to scatterometry', J. Geophys. Res. 92,4971-5029 (1 987).

23. R. Kodis, 'A note on the theory of scattering from an irregular surface', IEEE Trans. Antennas and Propagation **AP-14,** 77-82 (1966).

24. D.E. Barrick, 'Rough surface scattering based on the specular point theory', IEEE Trans. Antennas and Propagation, **AP-16,** 449-454(1968).

25. B.M. Tsai and C.S. Gardner, 'Remote sensing of sea state using laser altimeters', Appl. Opt 21,3932-3940 (1982).

26. G.M. Hale and M.R. Querry, 'Optical Constants of Water in the 200pm to 20pm Wavelength Region', Appl. Opt. 12,555-563 (1973).

27. D. Friedman, 'Infrared characteristics of ocean water (1 .5-15 p),' Appl. Opt. 8, 2073-2078 (1969).

28. P.A. Hwang and O.H. Shemdin, 'The dependence of sea surface slope on atmospheric stability and swell conditions,' J. Geophys. Res. 93, 13,903-13912 (1988).

29. J.A. Shaw and J.H. Churnside, 'Scanning-laser glint measurements of sea-surface slope statistics.' Appl. Opt. 36,4202-4213 (1997).

30. R.W. Preisendorfer and C.D. Mobley, 'Albedos and Glitter Patterns of a Wind-Roughened Sea Surface', J. Phys. Oceanography **16, 1293-1316** (1986).

31. F.E. Hoge, W.B. Krabill, and R.M. SW-R, 'The reflection of airborne UV laser pulses from the ocean', Marine Geodesy 8, 313-344 (1984).

32. J.A. Weinman, 'Derivation of Atmospheric Extinction Profiles and Wind Speed Over the Ocean From a Satellite-Borne Lidar', Appl. Opt. 27,3994-4001 (1 9S8)

Table 1. LITE Landmark Track Opportunities

Location	Lat/Long	Day/Time (GMT)	Comments
Tropical Atlantic	9° N / 40° W	Day 255/17:37	Patchy clouds in FOV Intermittant signal loss
Gulf of California	310 NI 114° W	Day 255/23:42	No 1064 nm data
Tropical Eastern Pacific	10°S / 105° W	Day 257/20: 19	Signal saturation for small nadir angles
Gulf of California	27° N/111° W	Day 259/21 :46	
Lake Superior	47° N/88° w	Day 259/21:53	

FIGURE CAPTIONS

Figure 1. Modelled lidar reflectance from the sea surface for various wind speeds. Subsurface (underwater) volume backscatter is not included.

Figure 2. The lidar fractional reflectance increment with respect to incremental change in wind speed, for selected nadir angles.

Figure 3. LITE 355 nm backscatter from the Gulf of California Landmark Track, September 12, 1994, with model lidar reflectance curves for selected wind speeds. Saturated signal values at small nadir angles are not shown.

Figure 4. LITE 1064 nm backscatter from the tropical eastern Pacific Landmark Track, September 14, with model lidar reflectance curve for 5 m/s wind speed. Saturated signal values at small nadir angles are not shown

Figure 5. LITE 532 nm backscatter from the tropical eastern Pacific Landmark Track, September 14, with model lidar reflectance curve for 5 m/s wind speed. Saturated signal values at small nadir angles are not shown.

Figure 6. LITE 1064 nm backscatter from the Gulf of California Landmark Track, September 16, with model lidar reflectance curves for selected wind speeds.

Figure 7. LITE 532 nm backscatter from the Gulf of California Landmark Track, September 16, with model lidar reflectance curves for selected wind speeds.

Figure 8. LITE 1064 nm backseat ter from the Lake Superior Landmark Track, September 16, with model lidar reflectance curves for selected wind speeds.

Figure 9. LITE 532 nrn backscatter from the Lake Superior Landmark Track, September 16, with model lidar reflectance curves for selected wind speeds.

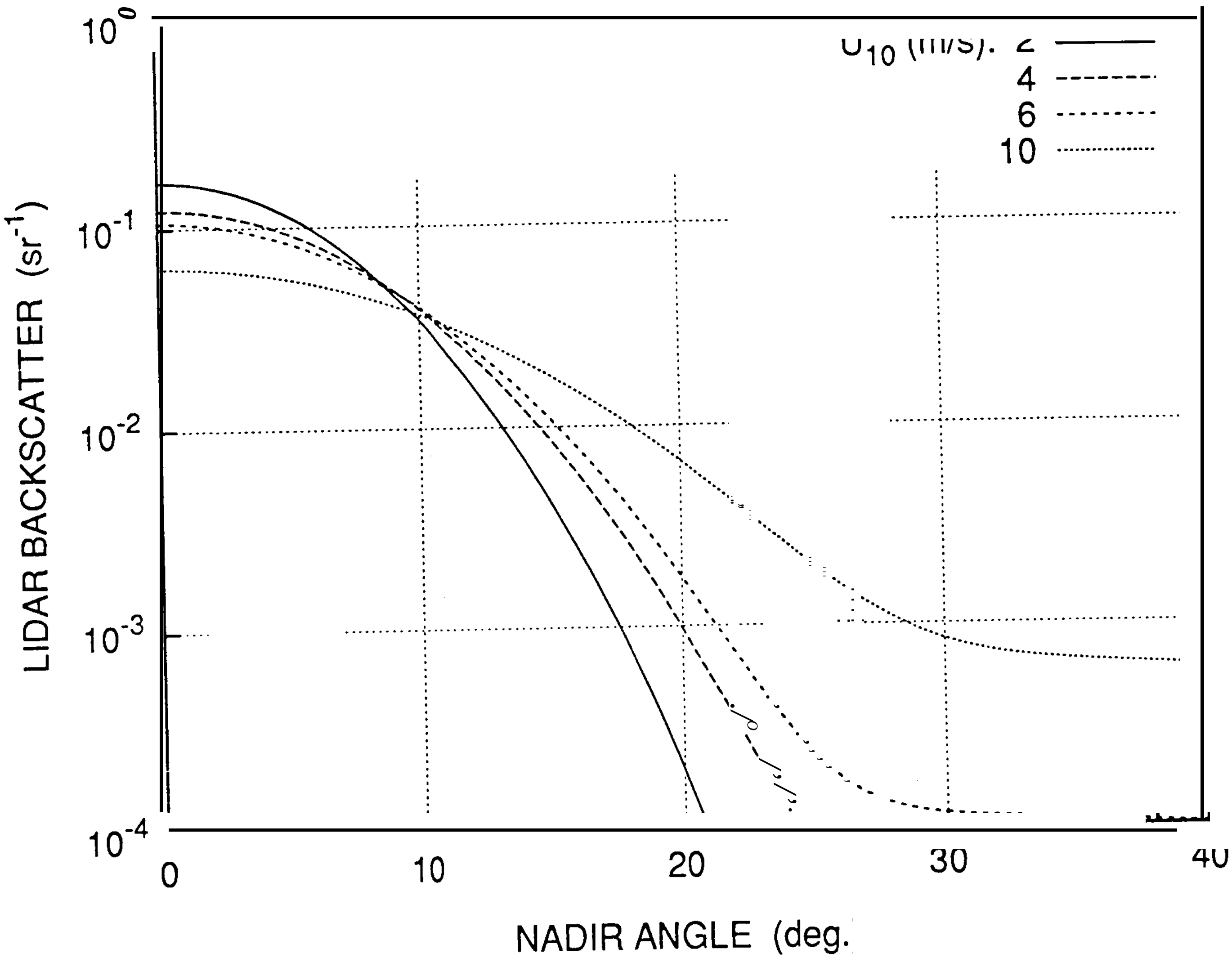
U_{10} (m/s): 2
4
6
10
LIDAR BACKSCATTER (sr^{-1})
10^{0}
10^{-1}
10^{-2}
10^{-3}
10^{-4}
0
10
20
30
40
NADIR ANGLE (deg.)

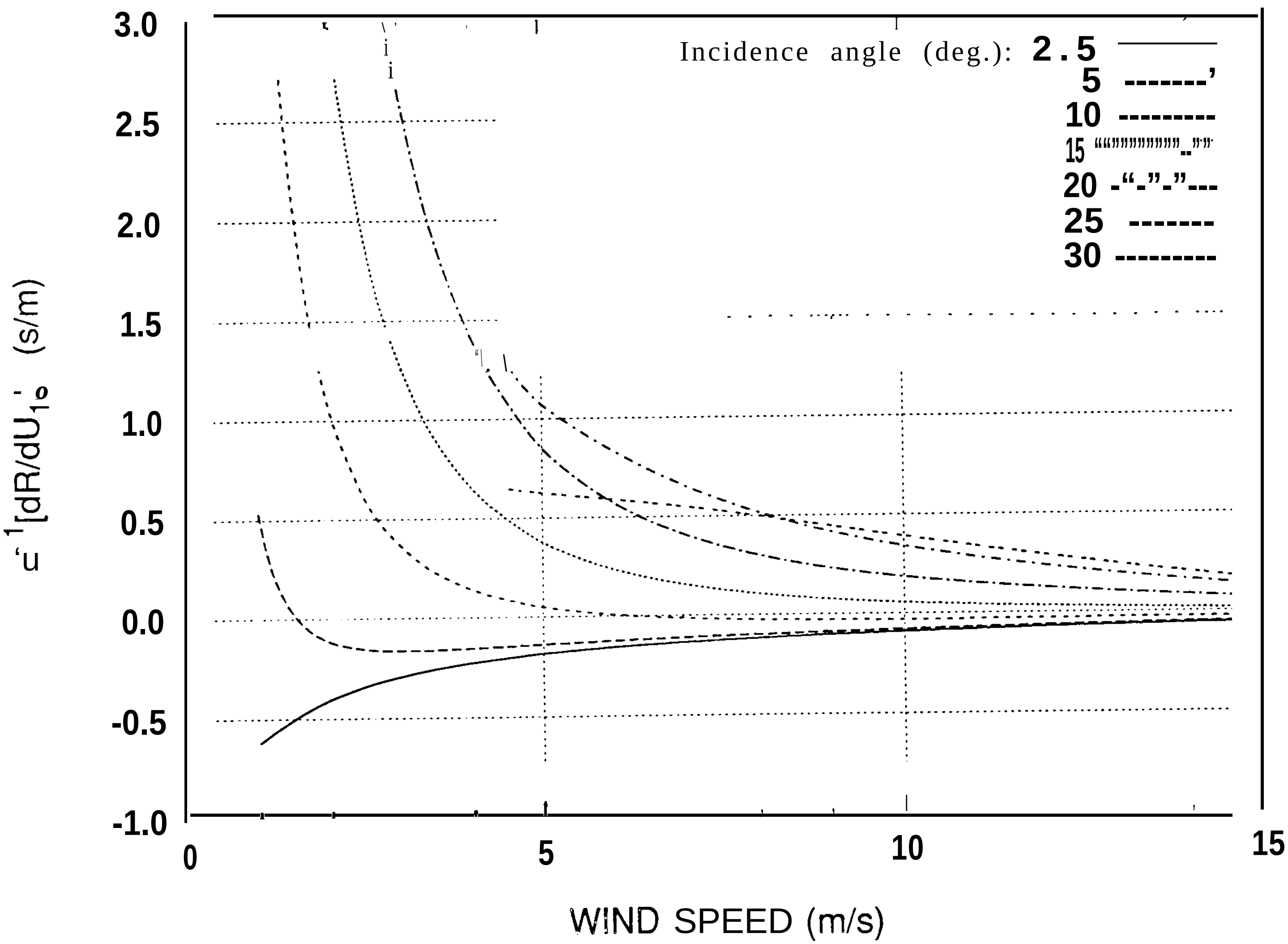

Incidence angle (deg.): 2.5
5
10
15
20
25
30
3.0
2.5
2.0
1.5
1.0
0.5
0.0
-0.5
-1.0
0
5
10
15
WIND SPEED (m/s)
(s/m)

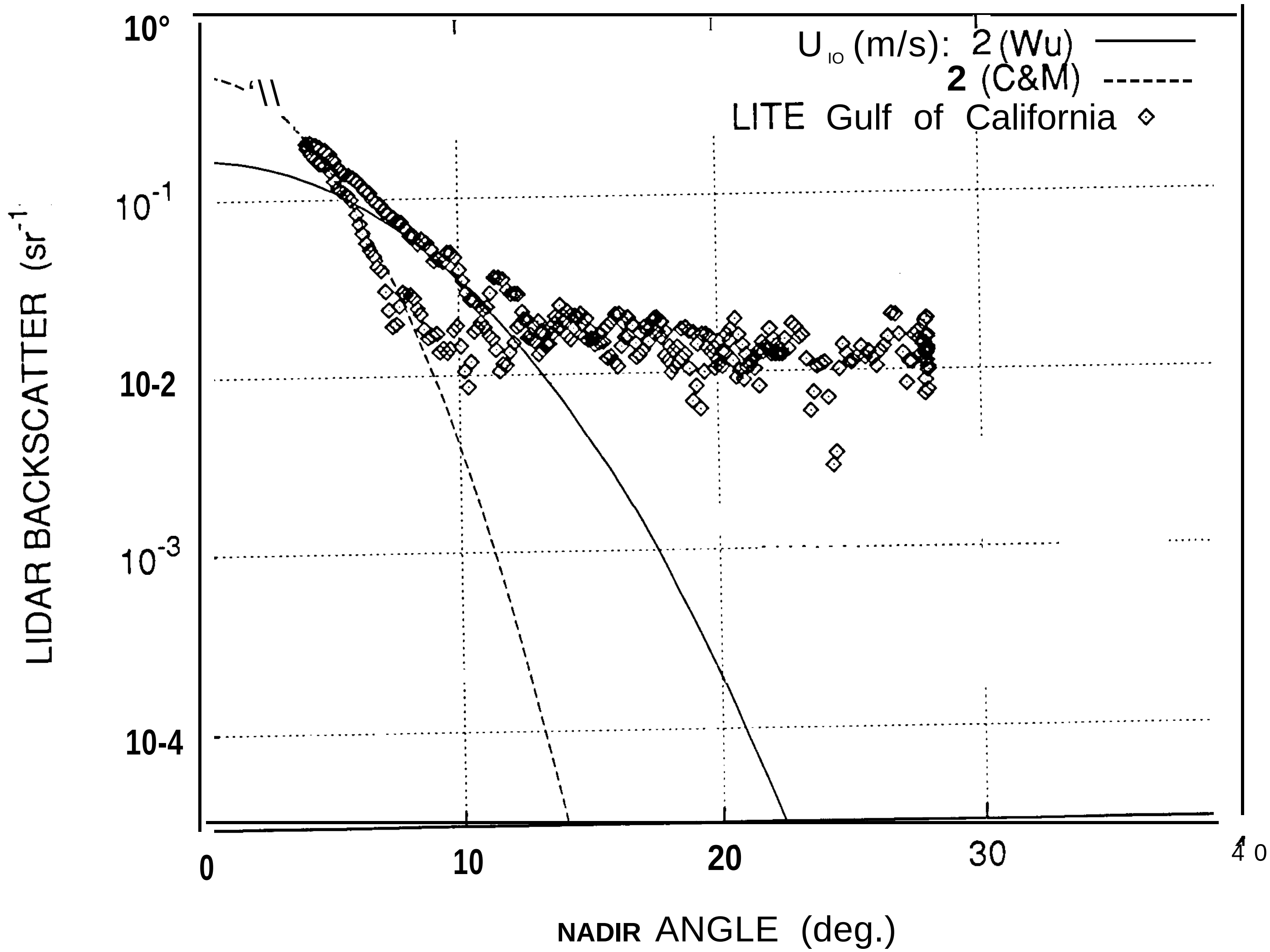

U_{10} (m/s): 2 (Wu)
2 (C&M)
LITE Gulf of California
LIDAR BACKSCATTER (sr^{-1})
10^0
10^{-1}
10^{-2}
10^{-3}
10^{-4}
0
10
20
30
40
NADIR ANGLE (deg.)

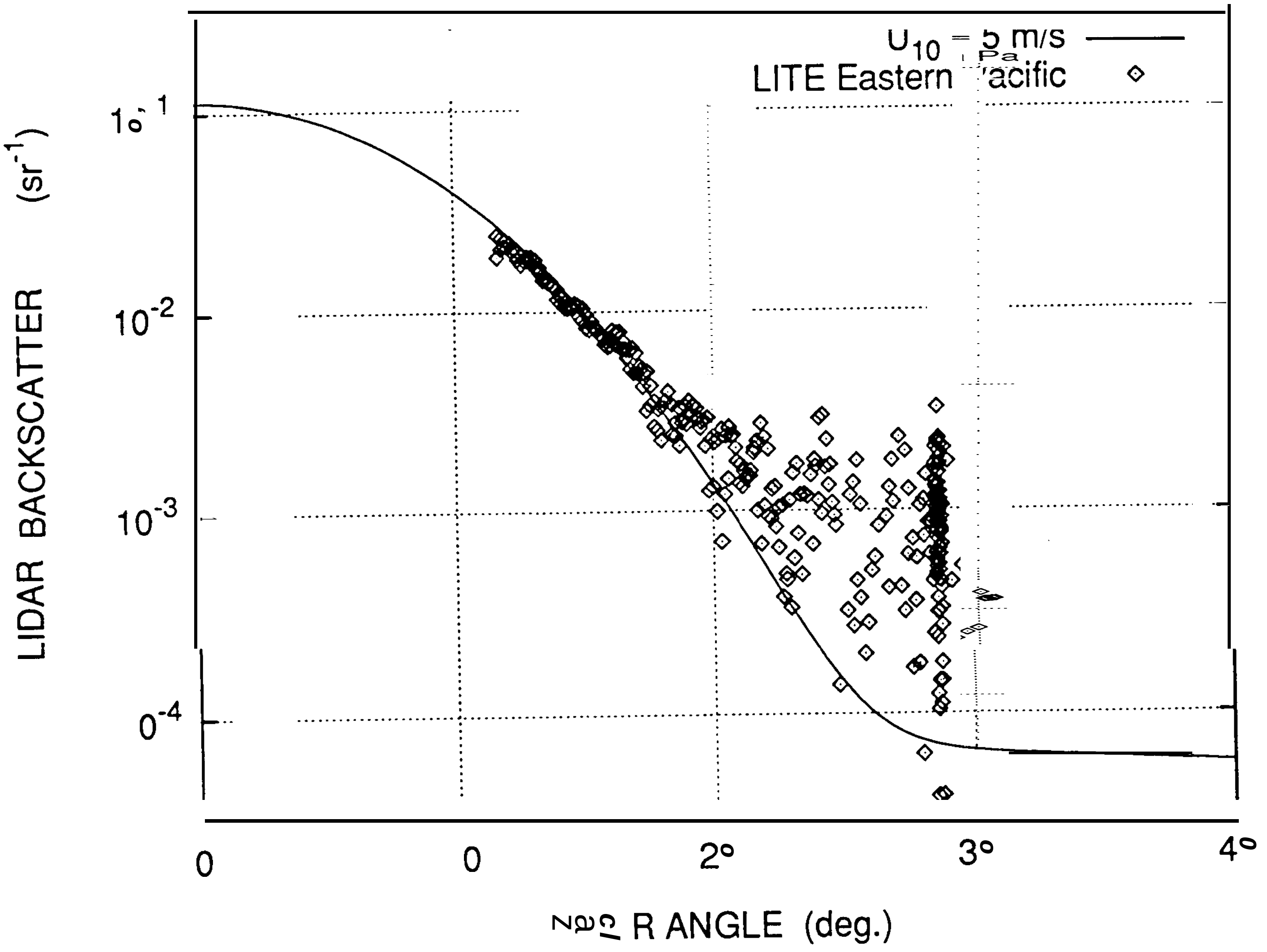

LIDAR BACKSCATTER (sr^-1)
10^-1
10^-2
10^-3
0^-4
0
0
2°
3°
4°
R ANGLE (deg.)
U10 = 5 m/s
LITE Eastern 'acific

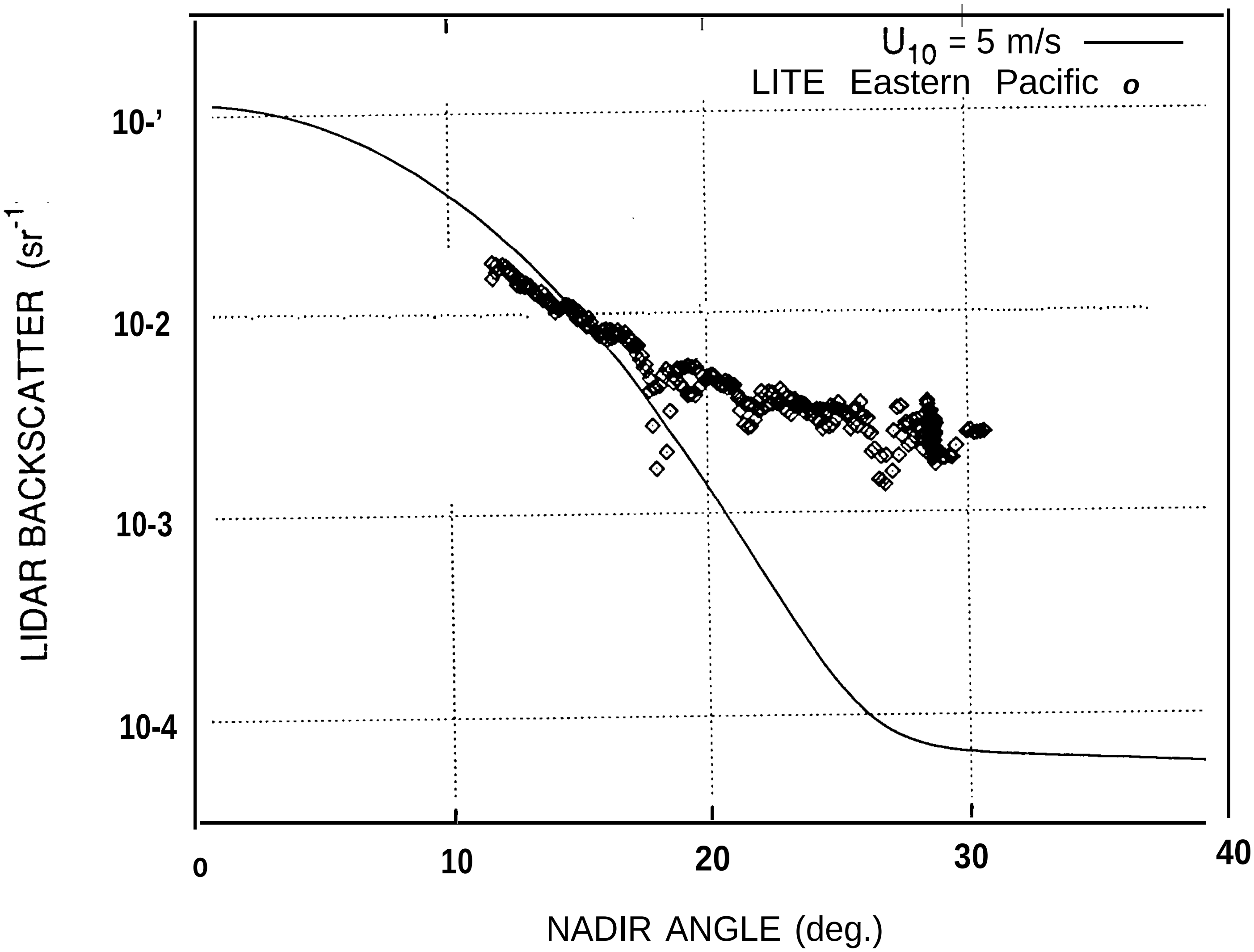

U10 = 5 m/s
LITE Eastern Pacific o
10-'
10-2
10-3
10-4
LIDAR BACKSCATTER (sr-1)
0
10
20
30
40
NADIR ANGLE (deg.)

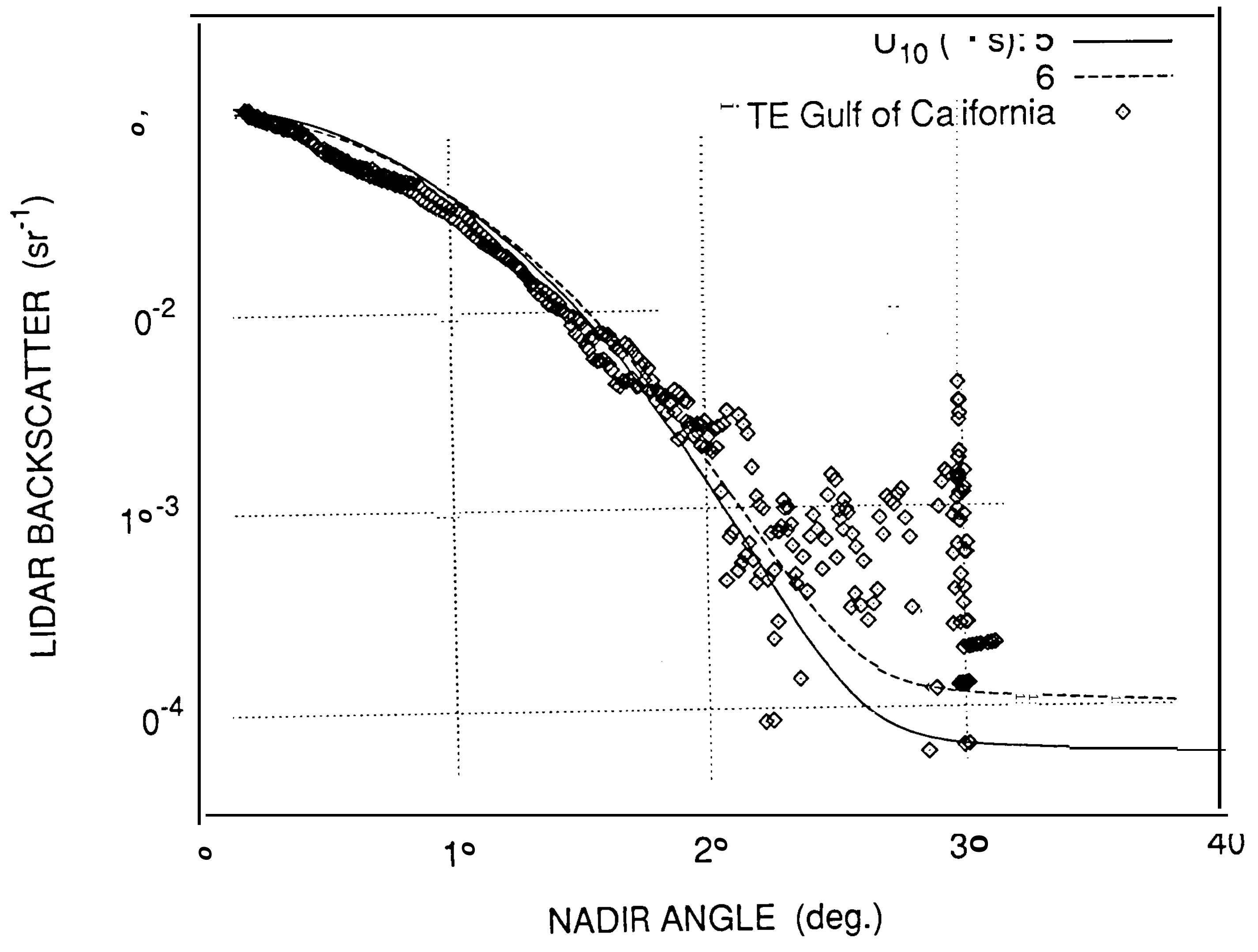
U10 (· s): 5
6
TE Gulf of Ca ifornia
LIDAR BACKSCATTER (sr-1)
0-2
1o-3
0-4
o
1o
2o
3o
40
NADIR ANGLE (deg.)

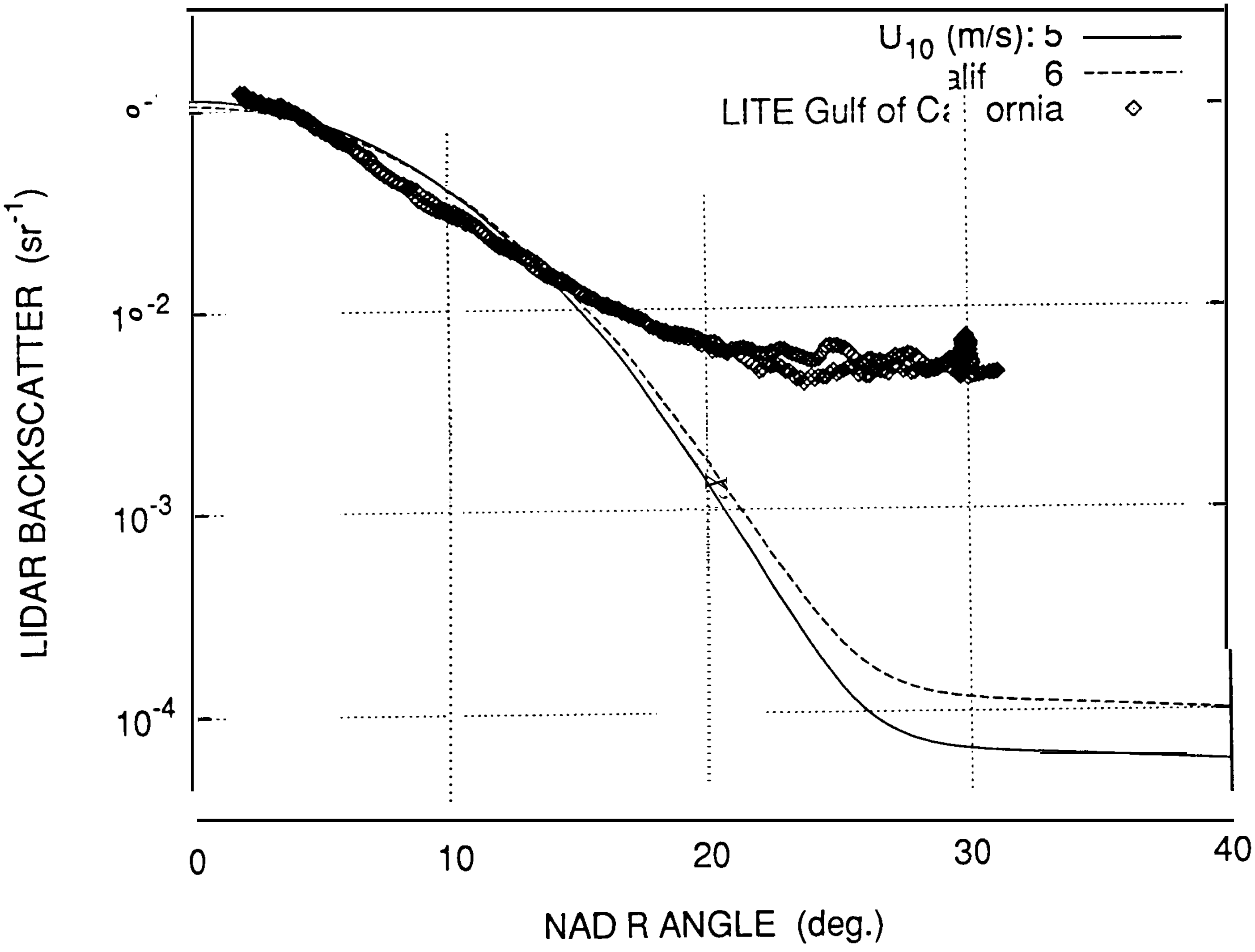

U10 (m/s): 5
6
LITE Gulf of California
LIDAR BACKSCATTER (sr-1)
10-2
10-3
10-4
0
10
20
30
40
NAD R ANGLE (deg.)

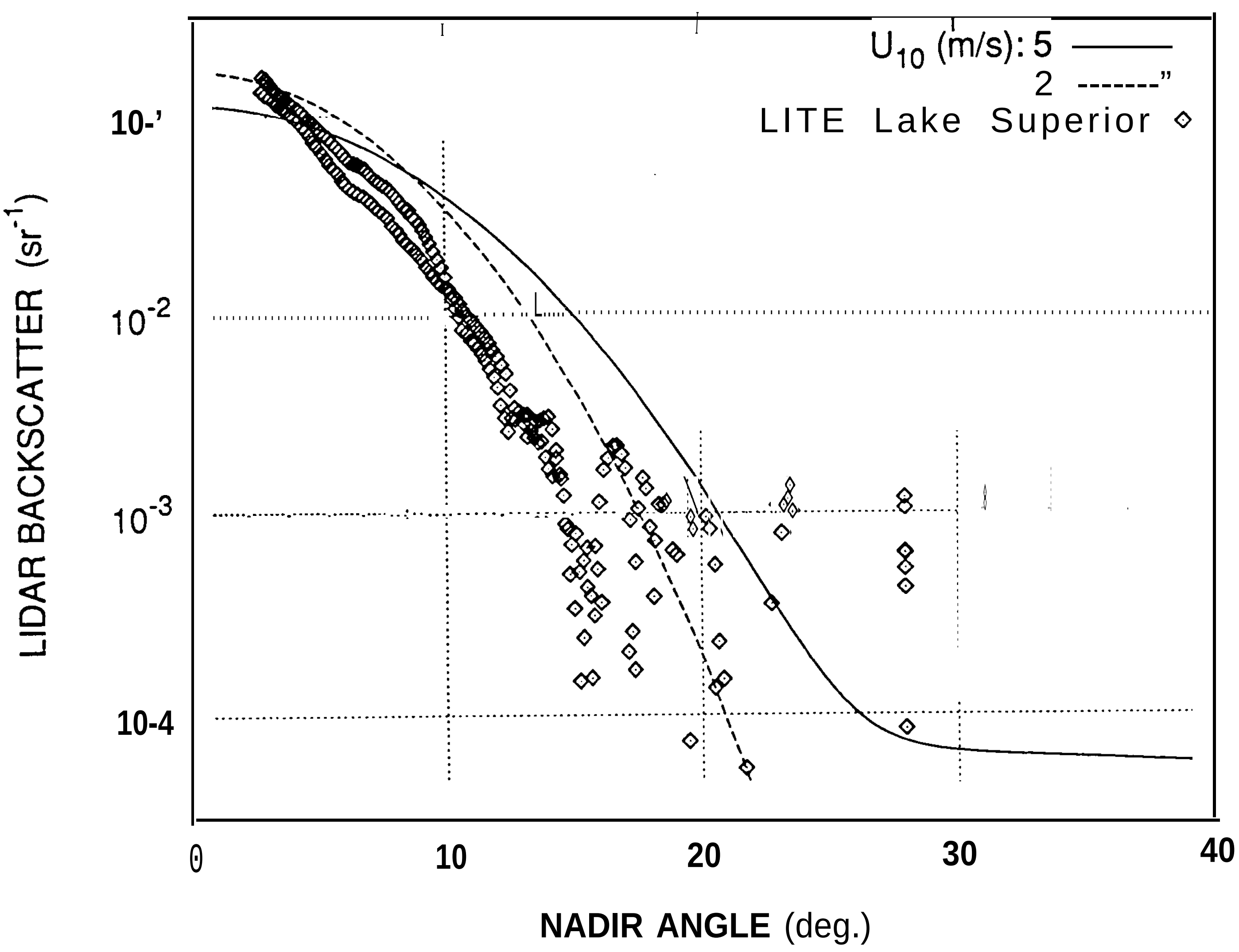

U10 (m/s): 5
2
LITE Lake Superior
10-'
10-2
10-3
10-4
LIDAR BACKSCATTER (sr-1)
0
10
20
30
40
NADIR ANGLE (deg.)

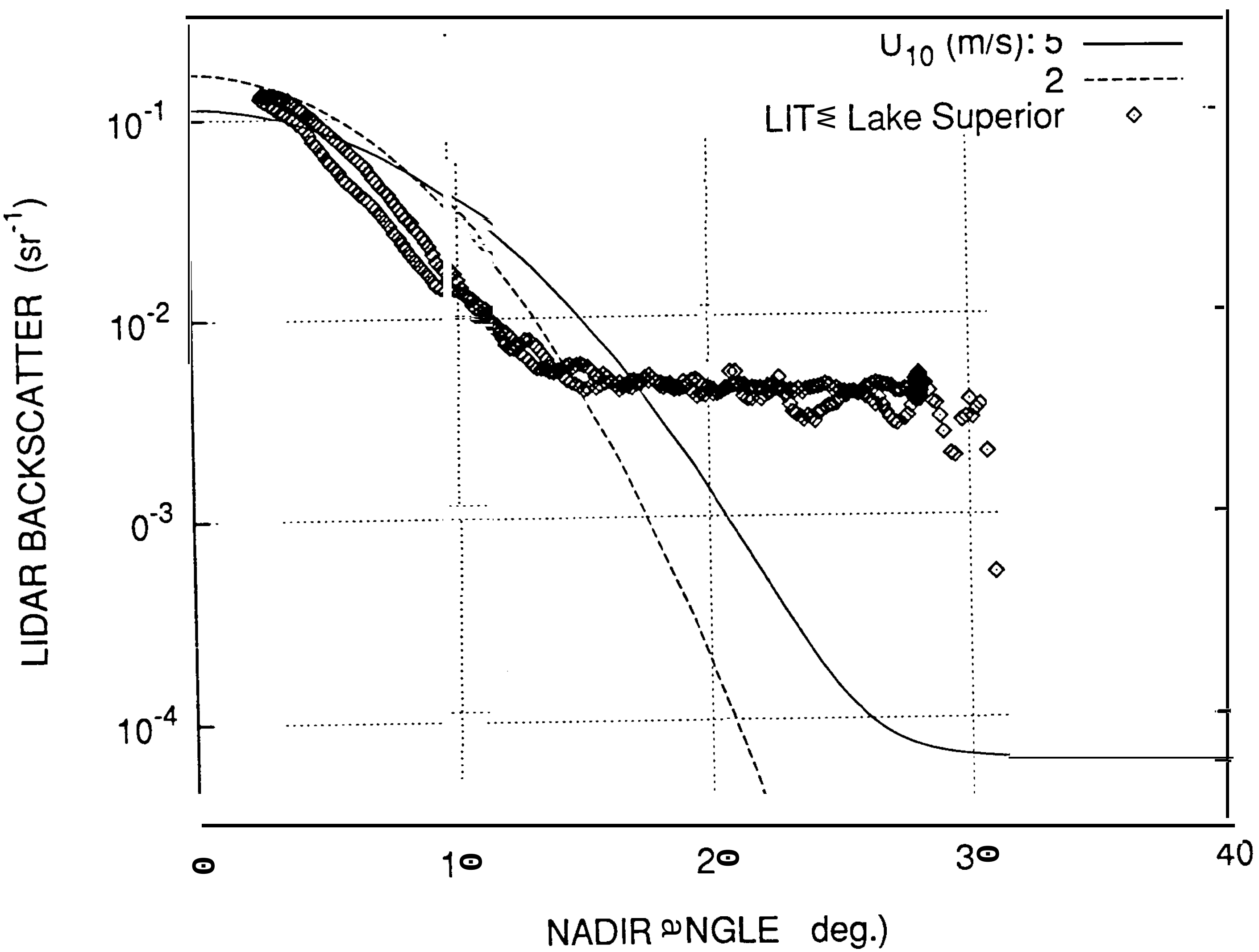

U10 (m/s): 5
2
LIT Lake Superior
10-1
10-2
0-3
10-4
LIDAR BACKSCATTER (sr-1)
0
10
20
30
40
NADIR ANGLE deg.)